RSC Advances

ROYAL SOCIETY OF CHEMISTRY

www.rsc.org/advances

Non-linear viscoelastic properties of TATB-based polymer bonded explosives modified by neutral polymeric bonding agent

Congmei Lin,[a] Jiahui Liu,[a] Guansong He,[a] Luoliang Chen,[b] Zhong Huang,[a] Feiyan Gong,[a] Yonggang Liu,[a] Shijun Liu *[a]

The neutral polymeric bonding agent (NPBA) was selected to enhance the interface adherence between 1,3,5-triamino-2,4,6-trinitrobenzene (TATB) crystals and fluoropolymer. The interfacial performance of the composites was investigated by the measurement of contact angle and the interfacial bonding mechanism was studied by XPS analysis. The results indicate that the hydrogen bond between TATB and NPBA is formed. The mechanical analysis of the TATB-based polymer bonded explosives (PBXs) revealed that the storage modulus, the mechanical strength and elongation at break of the formulation modified by NPBA were improved. The creep behaviors of the TATB-based PBXs with and without NPBA were also investigated at different temperatures and stresses. Reduced creep strain and steady-state creep strain rate and prolonged creep failure time were observed for the modified formulation, suggesting enhanced creep resistance performance. The creep experimental data was evaluated using a six-element mechanical model and the long-term creep performance of the materials was predicted using the time-temperature superposition principle. The creep behavior up to 6.0 years at 30 °C/4 MPa could be predicted by the short-term experimental data (5400 s) acquired at 30~80 °C under 4 MPa. The application of NPBA provides an efficient route to reinforce, toughen, and improve creep resistance of the explosive composites, such as TATB-based PBXs in this study.

1. Introduction

In recent years, polymer bonded explosives (PBXs) are extensively applied in military field ranging from rocket propellants to the explosive charge.[1-5] During storage and transportation, PBXs are subject to various loads and prone to deformation and damage from micro-cracks initiated from widely distributed manufacturing defects within the material.[6] Therefore, the inspection of mechanical response in PBX subject to external load is of great importance for characterizing of the material as well as for the design of new PBXs.

Generally, PBX is a kind of particle highly filled composite material which is comprised of 90-95% weight of explosive crystals and 5-10% weight of a polymeric binder.[7] As a multicomponent material, PBX consists of several phases in which interfaces exists between the phases. It is now well accepted that the mechanical response of PBX is dependent on the components, such as explosive crystal and polymer binder, and the interfacial interactions.[8-10] With confirmed components and phase morphology for a certain PBX, the interfacial interactions play a key role in particulate filled polymer.

Due to the interfacial debonding that occurs between the explosive particles and polymer matrix,

[a]Institute of Chemical Materials, China Academy of Engineering Physics, Mianyang, Sichuan 621900, P. R. China.
[b]Liming Research Institute of Chemical Industry, Luoyang, Henan 471001, P. R. China.
E-mail: lsj99@sohu.com, Fax: +86-816-2495856; Tel: +86-816-2482005.

the nucleation of micro-voids takes place, resulting in the final fracture in PBX.[11-14] Recognition of the role of the surface modification influencing interfacial adhesion is of utmost importance for the research and development of PBX. Consequently, many attempts have been made to improve the interfacial bonding of the explosive particles and polymer matrix. It has been reported that some parts of 1,3,5-triamino-2,4,6-trinitrobenzene (TATB) particle surface are activated and the surface modification is achieved by physics methods, including microwave and ultraviolet ray irradiation, with strengthened the wetting ability and the interactions with polymer binder.[15] The introduction of coupling agents has been proved to be an economical, rapid, and versatile way to obtain enhanced interfacial bonding properties. With the addition of neutral polymeric bonding agent (NPBA), the interface adherence between crystals with fluoridated binder in HMX-based PBX is enhanced, leading to improved creep resistance performance and tensile strength.[16]

Because of the extraordinary stability under thermal, impact, or shock-initiation conditions, TATB is commonly used in PBXs.[17-20] On the other hand, fluoropolymer is one kind of the most commonly used binders with good physical and chemical stability, excellent aging resistance and heat resistance.[21-23] The blending of TATB and fluoropolymer, such as LX-17 (92.5% TATB and 7.5% kel-F800 by weight) and PBX-9502 (95% TATB and 5% kel-F800 by weight), provides an effective way to make full use of their respective advantages and has been widely investigated in the academic and industrial fields.[24-26] However, the significant inter- and intramolecular hydrogen bonding results in the very low surface energy and poor adhesive performance of TATB.[27,28] In addition, low intermolecular cohesion force, weak interfacial bonding with gas, and very low surface tension of fluoropolymer lead to very poor adhesion with other materials.[29-31] Several studies have focused on the characterization of adhesive properties between TATB and fluoropolymer both by theoretical and experimental investigation.[32-34] The adhesion properties of fluoro- and perfluoropolymers, such as Kel-F800, Teflon AF, Hyflon AD, and Cytop, onto TATB crystal surfaces are investigated by atomistic simulations. It has been revealed that all polymers except Hyflon have a propensity to readily wet the TATB [100] and [001] surfaces.[35] Li et al have reported that due to the formation of the hydrogen bond between amino group of the coupling agents and nitro-group of TATB, and coordination bond between boric atom of the coupling agents and fluorine atom of fluoropolymer, the interfacial bonding of fluoropolymer/TATB is improved remarkably with the addition of coupling agents.[36]

Incorporation of bonding agent into polymeric materials has been widely investigated over the past decades. However, a comprehensive understanding of the influence of bonding agent on the interfacial interaction between TATB and fluoropolymer and the mechanical response of PBX subject to combined thermal and mechanical loads is lacking. In this article, a neutral polymeric bonding agent was applied to study its effects on interfacial interaction, mechanical behaviors, and the creep relaxation process of TATB-based PBXs. In addition, morphological characterization was carried out to study the failure mechanism of PBXs.

2. Experimental Section

2.1 Materials

1,3,5-triamino-2,4,6-trinitrobenzene (TATB) with 97% purity was provided by Institute of Chemical Materials, CAEP, China. Fluoropolymer used as polymer binder in this work is a copolymer of chlorotrifluoroethylene and vinylidene fluoride, purchased from Zhonghao Chenguang Chemical Industry Co., Ltd. China. Neutral polymeric bonding agent (labeled as

LBA-02) which was prepared by polymerization from 5, 5-dimethylhydantoin as the host material, acrylonitrile (AN) and methylmethacrylate (MMA) as the main monomers, as shown in reaction equation (1), was obtained from Liming Research Institute of Chemical Industry, China. The composition of LBA-02 was analyzed by FTIR, as shown in Fig. 1. The absorbance peaks at 1689.34 and 3450.03 cm^{-1} attributed to the C=O stretching vibration $\nu_{C=O}$ and N-H bending vibration δ_{N-H} of –CO-NH- group. The peaks at 1735.62 cm^{-1} which represent the C-O stretching vibration $\nu_{C=O}$ spectrum peak confirm the fact that –COO- group exists in LBA-02. The peak at 2242.81 cm^{-1} is attributed to the characteristic absorbance of -C≡N groups.

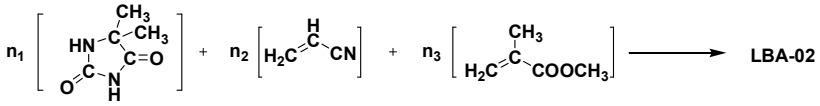

(1)

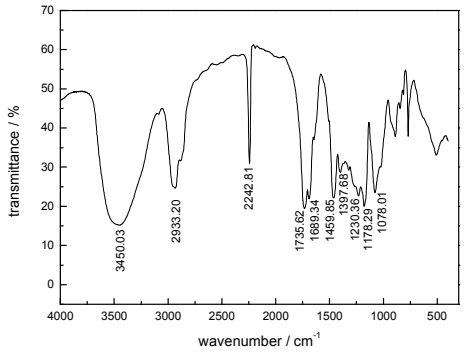

Fig. 1 The IR curves of neutral polymeric bonding agent (LBA-02).

2.2 Sample Preparation

In order to obtain the infrared spectra and X-ray photoelectron energy spectra, the surface treatment of TATB was conducted. TATB (2 g), 0.005 g LBA-02, and 10 mL acetone were added to a flask, and stirred for 10 min. After filtrating and washing, TATB was dried under vacuum.

Water suspension methods were applied to prepare the molding powders for TATB-based PBXs with or without NPBA.[19] The molding powders were dried in a vacuum oven at 60 °C for 24 h before the mould pressing process. Subsequently, the molding powders were pressed into grains for mechanical and creep test.

2.3 Measurements

The contact angles of test fluids on the surface of TATB pellet, fluoropolymer film, and neutral polymeric bonding agent film were measured by TY-82 contact angle instrument. Distilled water, glycerol, and diodomethane were selected as test fluids for contact angle measurements.

VG 250 X-ray photoelectron energy spectrum with monochromatic Mg-K_a X-rays was used to detect the change of electron binding energy of elements on the TATB surface.

Dynamic mechanical analysis (DMA) with specimen dimensions of 30 mm × 10 mm × 1~2 mm (length × width × thickness) was conducted with a DMA 242C apparatus (Netzsch, Germany) in three-point bending mode at a frequency of 1 Hz. The heating rate was set for 1 °C/min.

All static mechanical tests were performed with a universal testing machine (5582, INSTRON, USA). At least three specimens of each PBX were tested, and the average values were reported.

CamScan Apollo 300 (UK) scanning electron microscopy was adopted to observe the fracture morphology of PBXs.

The three-point bending creep test was conducted using a dynamic mechanical analyzer (DMA 242C, Netzsch, Germany). The specimens were loaded for 5400 s and at four temperatures and three stress levels.

3. Results and Discussion

3.1 Interaction intensity between TATB, fluoropolymer and NPBA

On the basis of contact angle experiments, surface tensions of TATB, fluoropolymer and neutral polymeric bonding agent (NPBA) could be obtained by geometric equation.[37]

$$\gamma_L (1+\cos\theta) = 2[(\gamma_S^d \gamma_L^d)^{1/2} + (\gamma_S^p \gamma_L^p)^{1/2}] \quad (1)$$

where γ_L is surface tension of liquid; θ is contact angle; γ_L^d and γ_L^p are dispersion component and polarity component of liquid, respectively; γ_S^d and γ_S^p are dispersion component and polarity component of solid, respectively.

The surface tension is constituted of dispersion component and polarity component.[38,39]

$$\gamma_S = \gamma_S^d + \gamma_S^p \quad (2)$$

The calculated surface tension for TATB, fluoropolymer and NPBA are listed in Table 1. For the material with low surface tension, the interfacial energy can be calculated by harmonic average equation:[36]

$$\gamma_{12} = \gamma_1 + \gamma_2 - \left[4\gamma_1^d \gamma_2^d / \left(\gamma_1^d + \gamma_2^d\right) + 4\gamma_1^p \gamma_2^p / \left(\gamma_1^p + \gamma_2^p\right)\right] \quad (3)$$

where γ_{12} represents the interfacial energy, γ_1 and γ_2 describe the surface tension of two phases, the superscripts d and p are dispersion component and polarity component, respectively.

And the adhesive work W_a could be determined by the following equation:

$$W_a = \gamma_1 + \gamma_2 - \gamma_{12} \quad (4)$$

The calculated interfacial energy and adhesion work of TATB/fluoropolymer and TATB/NPBA composites are summarized in Table 2. The interface adhesion work between power particles and the binder reflects the adhesion strength. It can be seen that the adhesion work between NPBA and TATB is bigger than that between fluoropolymer and TATB. The results indicate that compared to fluoropolymer, NPBA are easier to be bonded on the surface of TATB with a stronger interaction.

Table 1 Surface energies of TATB, fluoropolymer and NPBA

sample	γ^p / mN.m^{-1}	γ^d / mN.m^{-1}	γ / mN.m^{-1}
TATB	2.8	47.2	50.0
fluoropolymer	1.1	28.6	29.7
LBA-332	5.0	34.8	39.8

Table 2 Interfacial adhesive work between TATB, fluoropolymer and NPBA

sample	γ_{12} / mJ.m^{-2}	W_a / mJ.m^{-2}
TATB/fluoropolymer	5.31	74.39
TATB/NPBA	2.50	87.30

3.2 XPS

The change of electron binding energy of elements on the TATB surface can be detected through XPS tests, providing valuable insight into the bonding mechanism of particle-matrix interface.

The XPS spectra of TATB surface N1s elements are summarized in Fig. 2. From the N1s spectra of TATB, it can be seen that TATB exists three peaks centered at 397.14 eV, 402.79 eV, and 405.64 eV, respectively. The main peak centered at 397.14 eV corresponds to the nitrogen in -NH_2 group. Another main peak centered at 402.79 eV and a secondary peak at 405.64 eV belong to the nitrogen in -NO_2 group, in accordance with the results as reported recently.[19] As illuminated in Fig. 2, with the addition of very low content of NPBA, the electron binding energies of N atom on nitro-group of TATB decrease from 402.79 eV and 405.64 eV to 402.54 eV and 405.49 eV and the electron binding energies of O atom on nitro-group of TATB decrease from 529.84 eV to 529.69 eV, indicating an electrophilic effect of TATB from NPBA. Due to the induction effect of the benzene ring, the electron binding energies of N belonging to amino-group of TATB also decrease from 397.14 eV to 396.99 eV. The formation of hydrogen bond between TATB and NPBA is facilitated by the decreasing trend of the electron bonding energy of oxygen atom of TATB, and the hydrogen atom in -CO-NH- group of NPBA may form hydrogen bond with oxygen atom in -NO_2 group of TATB.[36] These results are also in good accordance with the contact angle analysis as mentioned above.

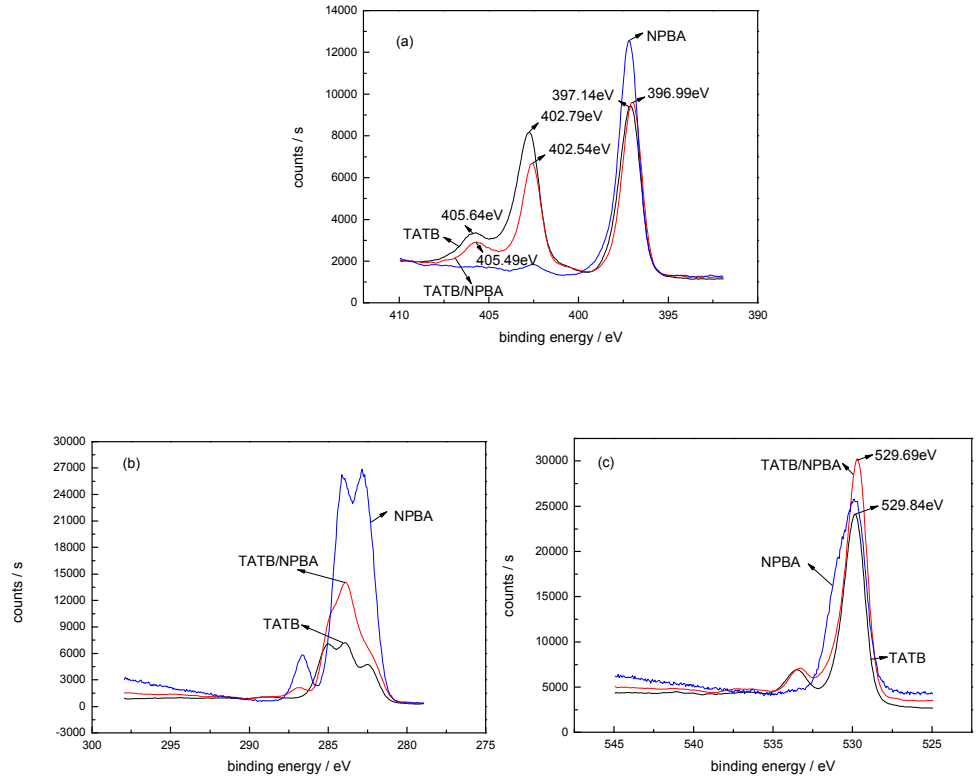

Fig. 2 XPS spectra for TATB, NPBA and TATB/NPBA composites. (a) N1s; (b) C1s; and (c) O1s.

3.3 Mechanical properties

Fig. 3 shows the dependence of the storage modulus (E') and loss factor (tanδ) on the temperature for TATB-based PBXs. It can be seen that the storage modulus gradually decreases within the experimental temperature range, and then begins to abruptly decline (Fig. 3a), which is related to the glass transition of the polymer binder.[40] Comparing PBX-A without NPBA, the storage modulus is improved for PBX-B in the whole temperature range. The increase of the storage modulus can be attributed to the increased interactions between TATB and polymer chains with the presence of NPBA. After modification by the coupling agent, the dynamic mechanical tanδ peak became broader towards higher temperatures (Fig. 3b).

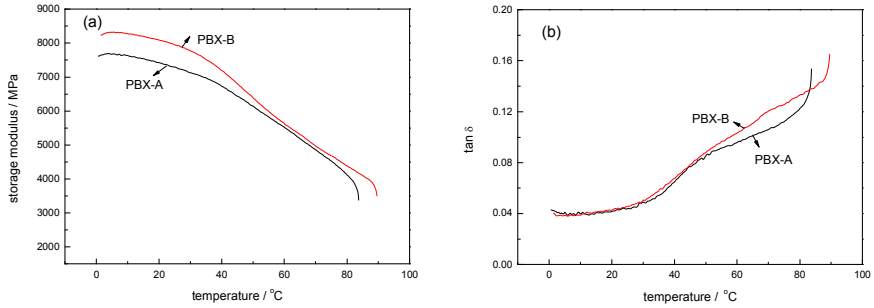

Fig. 3 Dynamic mechanical (a) storage modulus and (b) tanδ as a function of temperature for TATB-based PBXs.

Static mechanical tests, including compressive and Brazilian test were also conducted at room temperature. In case of specimens made from brittle materials, Brazilian disc test is the most convenient substitute of the direct tensile test to estimate the tensile properties with the advantage of little dosage and simplicity of specimen preparation。Fig. 4 reveals the representative stress-strain curves of two PBXs at room temperature. It is revealed that the compressive strength and tensile strength of PBX-B are raised by 13.7% and 48.3% compared to PBX-A, when NPBA is used. The results agree with the above DMA results. PBX-B has up to 33.2% and 130.1% higher compressive and tensile elongation at break than PBX-A, suggesting that PBX could be reinforced and toughened by the addition of NPBA. We believe that the higher interfacial strength between TATB and polymer matrix leads to better load transfer and fracture energy absorption, resulting in an efficient reinforcement and toughening effect in PBX-B.

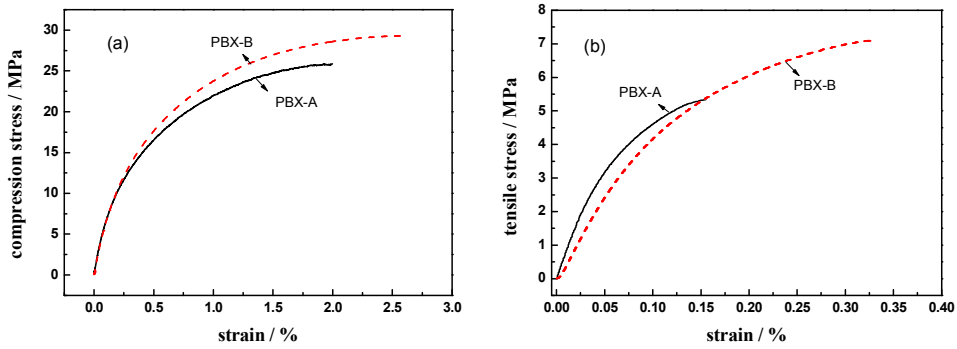

Fig. 4 The typical mechanical response for TATB-based PBXs at room temperature: (a) compressive test, (b) Brazilian test.

3.4 Morphology analysis

In order to analyze the fracture mechanism, the fracture surface obtained after dynamic mechanical measurement observed by SEM. During the dynamic mechanical measurement, the specimen was coinstantaneously affected by tensile loading, compressive loading, and elevated temperature. Fig. 5(a) and (b) present the SEM images of the fracture surface of PBX-A and PBX-B, respectively. In Fig. 5(a), it can be clearly seen that a lot of filamentous binder existed at the fracture surface of PBX-A, indicating that the rupture mode is mainly binder breakage. Some of the TATB particles experience cleavage fracture due to compression loading. Besides, some interfaces between the TATB particles and binder disbond because of extension. Therefore, the microscopic fracture mechanism is a combination of transcrystalline, intercrystalline rupture, and binder breakage under combined temperature and mechanical loading. For PBX-B, filamentous binder, the interfacial debonding, breaking of TATB particles are also observed, indicating the microscopic fracture mechanism would not change by NPBA. However, it should be emphasized that the amount and magnitude of filamentous binder evidently increase in the presence of NPBA. The results are attributed to the fact that the interfacial interaction between TATB particles and binder matrix is strongly enhanced for PBX-B, resulting in more binder breakage under combined temperature and force loading.

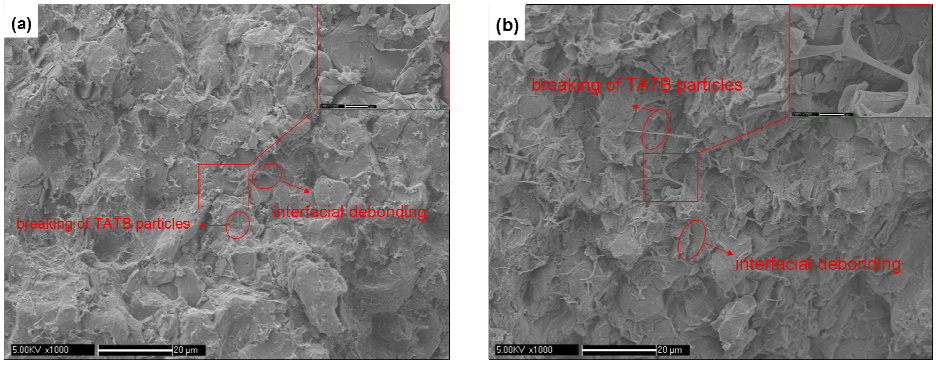

Fig. 5 SEM images of the fracture surface: (a) PBX-A, (b) PBX-B.

3.5 Three-point bending creep tests

3.5.1 Creep strain curves

The creep tests were applied to TATB-based PBXs at 60°C under different stresses for 5400 s. The time-dependent creep strain values for PBX-A and PBX-B samples are demonstrated in Fig. 6. In order to relate the different responses of TATB-based PBXs to the applied load, the creep performance parameters under different stresses at 60 °C, including the steady-state creep strain rate, maximal creep strain, and creep failure time of TATB-based PBXs, are listed in Table 3. Among the parameters, the steady-state creep strain rate is known to be a good indicator to determine the dimensional stability of polymer composites,[41] which is acquired from the slope of the linear fitting line of the steady-state creep stage in the creep strain curves (Fig. 7).

It was also seen from Fig. 6 and Table 3 that the creep strain values increase with increasing stress independent of the type of PBX. The creep behaviors of the PBX-A and PBX-B were not identical, especially under higher creep stresses, indicating the influence of NPBA on the viscoelastic properties of the PBXs. Under low stress (4 MPa), both PBX-A and PBX-B display a long-term creep process and no creep rupture time could be obtained. However, the PBX-B

exhibits lower creep strain and steady-state creep strain rate values than the PBX-A, indicating improved creep resistance of the PBX-B. Under higher loading stress (7 MPa), the creep failure of the sample PBX-A is occurred at 4155 s accompanied by large deformation, while PBX-B showed no significant characterization of the rupture. When the loading stress is further increased to 9 MPa, PBX-A and PBX-B involve the rupture at 660 s and 2610 s, respectively. A possible reason for this improvement is the increased interactions between TATB and polymer binder by NPBA.

The temperature dependence of the creep response of TATB-based PBXs in the range from 30 °C to 80 °C under a stress of 4 MPa is also studied, as shown in Fig. 8. The experimental results demonstrate that a prominent increase of the creep strain of TATB-based PBXs is achieved by the increase of temperature, indicating the increased mobility of the polymer binder at elevated temperatures.

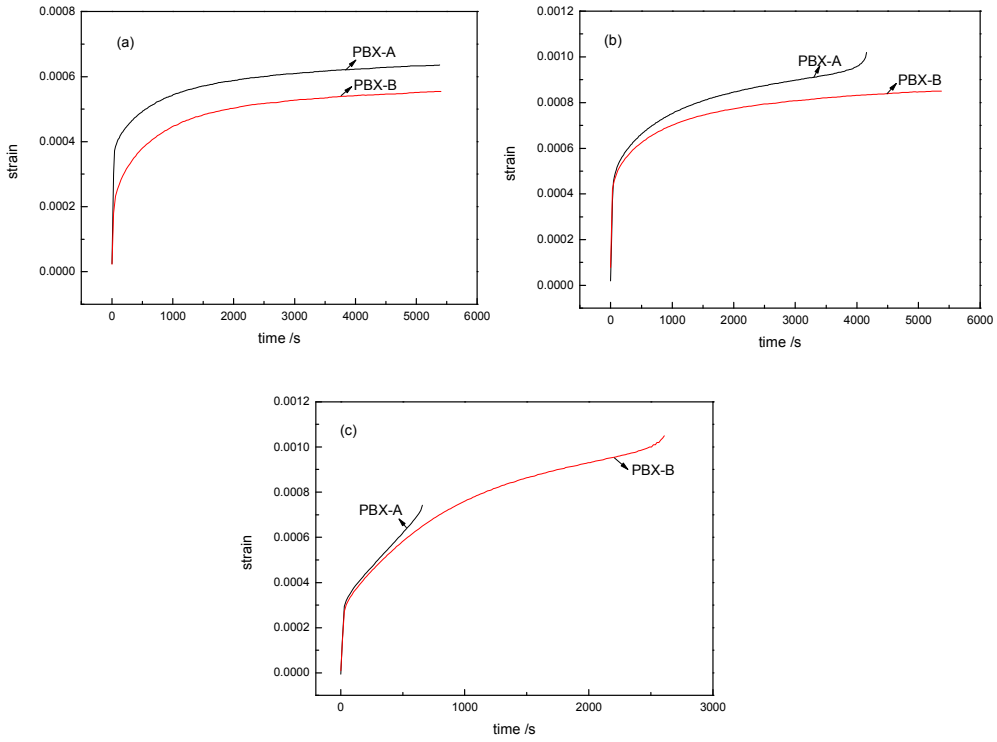

Fig. 6 Time-dependent creep strain of TATB-based PBXs under different stresses at 60 °C: (a) 4 MPa, (b) 7 MPa, (c) 9 MPa.

Table 3. The creep performance parameters of TATB-based PBXs under different conditions.

sample	experimental conditions	constant creep strain rate / s^{-1}	maximal creep strain	creep rupture time / s
PBX-A	60 °C/4 MPa	1.397×10^{-8}	6.356×10^{-4}	> 5400
	60 °C/7 MPa	5.152×10^{-8}	1.020×10^{-3}	4155
	60 °C/9 MPa	6.022×10^{-7}	7.423×10^{-4}	660
PBX-B	60 °C/4 MPa	1.212×10^{-8}	5.545×10^{-4}	> 5400
	60 °C/7 MPa	2.355×10^{-8}	8.511×10^{-4}	> 5400
	60 °C/9 MPa	1.225×10^{-7}	1.050×10^{-3}	2610

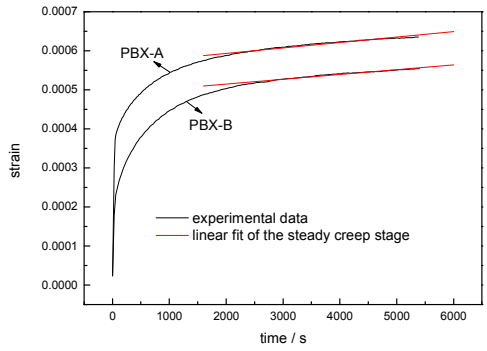

Fig. 7 The linear fit of the creep strain curves during steady creep stage of TATB-based PBXs at 60 °C/4 MPa.

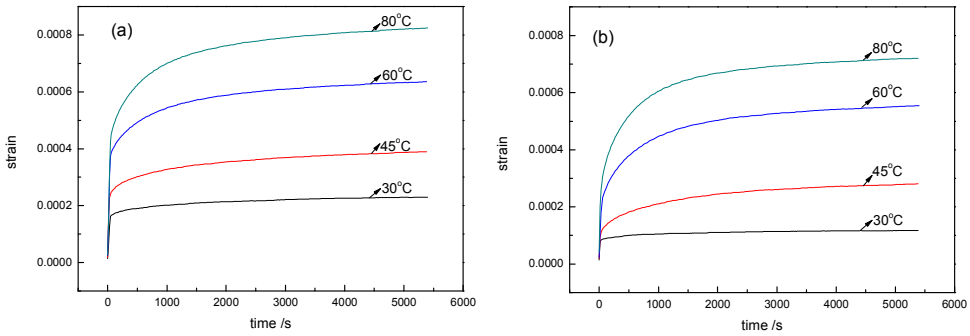

Fig. 8 Time-dependent creep strain of TATB-based PBXs at different temperatures under 4 MPa: (a) PBX-A, (b) PBX-B.

3.5.2 Creep modeling

The six-element mechanical model is successfully used to simulate the creep behavior of PBXs.[40] It consists of a consecutively connected Maxwell and two Kelvin units, as illustrated in Fig. 9. The total strain (ε) of polymer composite material PBX could be determined by the strains resulting from the Maxwell spring (ε_1), Maxwell dashpot (ε_4), and two Kelvin units(ε_2 and ε_3):

$$\varepsilon(t) = \varepsilon_1 + \varepsilon_2 + \varepsilon_3 + \varepsilon_4 = \frac{\sigma_0}{E_1} + \frac{\sigma_0}{E_2}\left(1 - e^{-t/\tau_2}\right) + \frac{\sigma_0}{E_3}\left(1 - e^{-t/\tau_3}\right) + \frac{\sigma_0}{\eta_4}t \qquad (5)$$

where ε(t) is the creep strain, σ_0 is the initial stress, E_1 is the elastic modulus of instantaneous elastic deformation, E_2 and E_3 are the elastic modulus of high elastic deformation, τ_2 and τ_3 are the relaxation time, η_4 is the bulk viscosity, respectively.

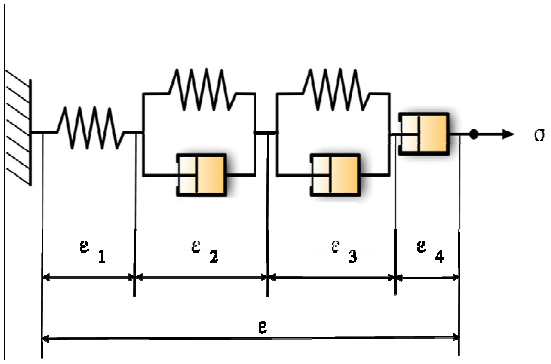

Fig. 9 Schematic representation of the six-element mechanical model.

The nonlinear curve fit function provided by Origin software is adopted to fit the experimental data of creep strain and the results are shown in Fig. 10. It can be seen that the modeling curves by the six-element mechanical model shows a satisfactory agreement with the experimental data at all temperatures examined with all square values of correlation coefficient R^2 greater than 0.994.

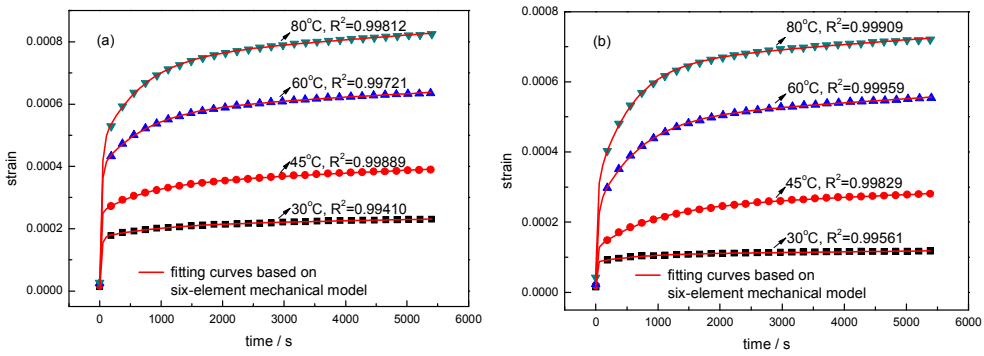

Fig. 10 Modeling results of creep behaviors of TATB-based PBXs at different temperatures under 4 MPa: (a) PBX-A, (b) PBX-B.

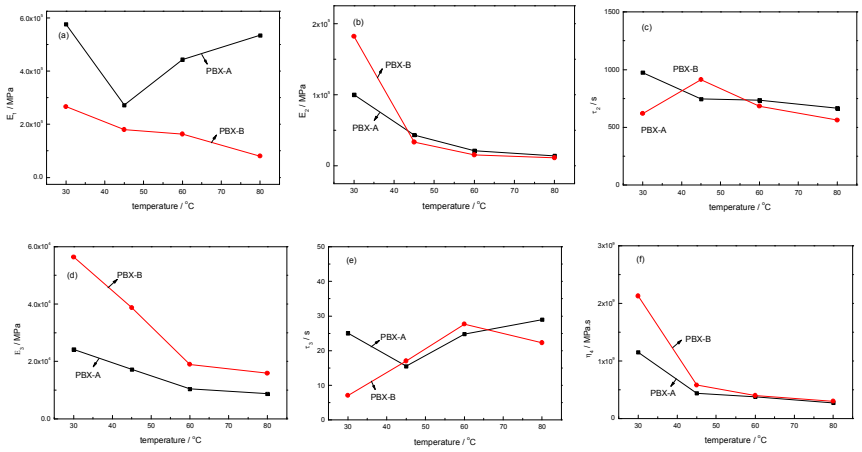

Fig. 11 Temperature dependence of the parameters in the six-element model.

The non-linear fitting parameters including the elastic modulus E_1, E_2, E_3, the relaxation time τ_2,

τ_3, as well as the bulk viscosity η_4 of TATB-based PBXs are extracted through direct modeling of the experimental creep data, as plotted as functions of temperature in Fig. 11. As can be seen from Fig. 11 that among fitting parameters, E_3 and η_4 decreased with increasing temperature for TATB-based PBXs. It can be found that the E_3 and η_4 values of PBX-B were higher than that of PBX-A, indicating the reinforcing effect of the NPBA on TATB-based PBX. E_3 is related to the spring in the Voigt unit, reflecting the mechanical properties of the amorphous regions. [41] η_4 is associated with the irrecoverable deformation of the materials. The increased values of η_4 indicate the reinforced resistance to viscous flow, which is attributed to the enhanced particle-matrix bonding by NPBA.

3.5.3 Prediction of long-term creep behaviors

Due to the limitations caused by performing creep experiment covering the entire service life time, the evaluation of long-term performance and durability for the application of PBX in weapon systems is difficult. Based on the time-temperature superposition principle (TTSP), long-term properties could be predicted by the short-term experimental data.[42] The creep behavior could be observed at a high temperature within a short time, also could be observed at a low temperature within a long time. For instance, the creep response at an elevated temperature is equivalent to one performed for an extended period of time. Consequently, a master curve could be constructed from the short term creep test data collected at different temperatures, providing a prediction for long-term performance of the PBXs.

The creep strain curve at reference temperature T_r and time t_r is received with a horizontal displacement of the creep strain curve at temperature T and time t:

$$D(T_r, t_r) = D(T_r, t / a_T) = D(T, t) \qquad (6)$$

where a_T is a shift factor. In this work, 30 °C is selected as the reference temperature for master curve of creep strain function. Fig. 12 depicts the three-point bending creep strain master curves as a function of creep time for TATB-based PBXs under 4 MPa. It is worth mentioning that PBX-B exhibits a lower value of predicted creep strain than that of PBX-A, illustrating the reinforcing effect of NPBA on the creep resistance of the material.

WLF equation is the special temperature dependence of the motion for chain segment:[43]

$$\log a_T = -\frac{C_1 (T - T_r)}{C_2 + (T - T_r)} \qquad (7)$$

where C_1 and C_2 are two coefficients. The shift factor a_T is obtained with the curve transformation and used to calculate the two coefficients C_1 and C_2 of WLF equation. The non-linear fit of shift factor $\log a_T$ versus temperature for TATB-based PBXs is presented in Fig. 13. The WLF equations fitting for PBX-A and PBX-B are $\log a_T = -\frac{8.25 (T - 303.15)}{37.87 + (T - 303.15)}$ and $\log a_T = -\frac{6.78 (T - 303.15)}{26.88 + (T - 303.15)}$, respectively. Based on the WLF equations, the horizontal displacement of the creep compliance curve at different temperatures to the reference temperature could be calculated.

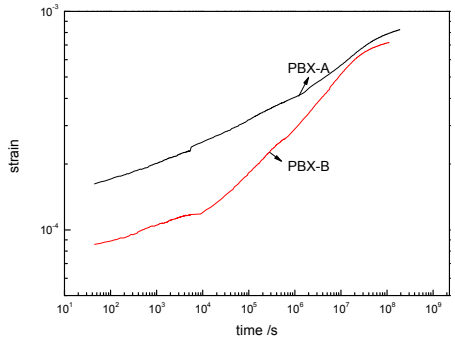

Fig. 12 Three-point bending creep strain master curves of TATB-based PBXs at a reference temperature of 30 °C.

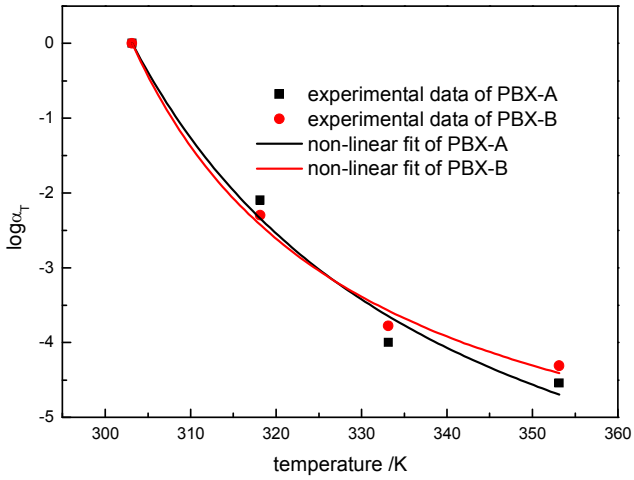

Fig. 13 The non-linear fit of $\log a_T$ versus temperature for TATB-based PBXs.

4. Conclusions

In this work, 1,3,5-triamino-2,4,6-trinitrobenzene (TATB)-based polymer bonded explosives (PBXs) were modified with a neutral polymeric bonding agent (NPBA). The contact angle and XPS experimental results revealed that the hydrogen bond between TATB and NPBA is formed, which confers to the material a higher mechanical performance. The observed decrease in the creep strain and steady-state creep strain rate and increase in creep failure time had been associated with the enhanced surface interactions between explosive crystals and polymeric binders by the introduction of NPBA into the TATB-based PBXs. Parameters extracted from the simulation with a six-element mechanical model indicated that the mechanical properties of the amorphous regions and permanent flow resistance of the TATB-based PBXs were reinforced by the presence of NPBA. Based on time-temperature superposition principle, the creep strain master curves were obtained at a reference temperature of 30 °C. The creep resistance performance is enhanced after interface modification with a downward shift of creep strain master curve. The experimental results indicated that interfacial interactions play a key role in the multicomponent

materials, such as TATB-based PBXs. The incorporation of NPBA is an effective approach to reinforce the viscoelastic properties of the TATB-based PBXs, including the storage modulus, the static mechanical properties and creep resistance.

References

1. M. L. Hobbs and M. J. Kaneshige, *J. Chem. Phys.,* 2014, **140**, 124203.
2. J. W. Tringe, J. R. Kercher, H. K. Springer, E. A. Glascoe, H. W. Levie, P. Hsu, T. M. Willey, and J. D. Molitoris, *J. Appl. Phys.,* 2013, **114**, 043504.
3. T. Li, C. Hua, and Q. Li. *Propell. Explos. Pyrot.*, 2013, **38**, 770-774.
4. M. B. Talawar, A. P. Agarwal, M. Anniyappan, G. M. Gore, S. N. Asthana, and S. Venugopalan, *J. Hazard. Mater.*, 2006, **137**, 1848-1852.
5. H. L. Berghout, S. F. Son, C. B. Skidmore, D. J. Idar, and B. W. Asay, *Thermochim. Acta*, 2002, **384**, 261-277.
6. X. Wang, S. Ma, Y. Zhao, Z. Zhou, and P. Chen, *Polym. Test.*, 2011, **30**, 861-866.
7. P. W. Cooper and S. R. Kurowski, Introduction to the Technology of Explosives, New York: Wiley-VCH, p.21-23, 1996.
8. P. Chen, H. Xie, F. Huang, T. Huang, and Y. Ding, *Polym. Test.*, 2006, **25**, 333-341.
9. Z. W. Liu, H. M. Xie, K. X. Li, P. W. Chen, and F. L. Huang, *Polym. Test.*, 2009, **28**, 627-635.
10. B. Pukánszky, *Eur. Polym. J.*, 2005, **41**, 645-662.
11. Z. Zhou, P. Chen, Z. Duan, and F. Huang, *Strain*, 2012, **48**, 326-332.
12. D. R. Drodge, D. M. Williamson, S. J. P. Palmer, W. G. Proud, and R. K. Govier, *J. Phys. D: Appl. Phys.*, 2011, **43**, 335403.
13. J. D. Yeager, M. Dubey, M. J. Wolverton, M. S. Jablin, J. Majewski, D. F. Bahr, and D. E. Hooks, *Polymer*, 2011, **52**, 3762-3768.
14. Q. An, W. A. Goddard III, S. V. Zybin, A. Jaramillo-Botero, and T. Zhou. *J. Phys. Chem. C*, 2013, **117**, 26551-26561.
15. X. Wang, H. Huang, and F. Nie, *Chinese J. Explos. Propell.*, 2001, **33**, 33-35.
16. J. Liu, S. Liu, L. Chen, C. Lin, F. Gong, and F. Nie, 45th International Annual Conference of the Fraunhofer ICT, 2014, P56/1-8.
17. C. Zhang, Y. Ma, and D. Jiang, *J. Mol. Model.*, 2012, **18**, 4831-4841.
18. R. H. Gee, S. Roszak, K. Balasubramanian, and L. E. Fried, *J. Chem. Phys.*, 2004, **120**, 7059-7066.
19. Z. J. Yang, J. S. Li, B. Huang, S. J. Liu, Z. Huang, and F. D. Nie, *Propell. Explos. Pyrot.*, 2014, **39**, 51-58.
20. J. T. Mang and R. P. Hjelm, *Propell. Explos. Pyrot.*, 2013, **38**, 831-840.
21. Q. L. Yan, S. Zeman, and A. Elbeih, *Thermochim. Acta*, 2013, **562**, 56-64.
22. D. M. Hoffman, *Polym. Eng. Sci.*, 2003, **43**, 139-156.
23. L. L. Stevens, D. M. Dattelbaum, M. Ahart, and R. J. Hemley, *J. Appl. Phys.*, 2012, **112**, 023523.
24. P. D. Peterson and D. J. Idar, *Propell. Explos. Pyrot.*, 2005, **30**, 88-94.
25. C. M. Tarver, *J. Phys. Chem. A*, 2010, **114**, 2727-2736.

26. P. Hsu, C. Souers, M. De Haven, R. Garza, J. Alvarez, and J. Maienschein, *J. Therm. Anal. Calorim.*, 2008, **93**, 311-317.
27. J. D. Yeager, A. M. Dattelbaum, E. B. Orler, D. F. Bahr, and D. M. Dattelbaum, *J. Colloid Interf. Sci.*, 2010, **352**, 535-541.
28. S. Roszak, R. H. Gee, K. Balasubramanian, and L. E. Fried, *Chem. Phys. Lett.*, 2003, **374**, 286-296.
29. B. Hopp, N. Kresz, J. Kokaveca, T. Smausz, H. Schieferdecker, A. Doring, O. Marti, and Z. Bor, *Appl. Surf. Sci.*, 2004, **221**,437.
30. T. R. Dargaville, G. A. George, D. J. T. Hill, and A. K. Whittaker, *Prog. Polym. Sci.*, 2003, **28**, 1355.
31. C. Lin, J. Liu, S. Liu, Z. Huang, Y. Li, J. Zhang, L. Pan, and J. Zhang, *Chinese J. Energ. Mater.*, 2014, **22**, 664-668.
32. T. Rivera and M. L. Matuszak, *J. Colloid Interf. Sci.*, 1983, **93**, 105-108.
33. H. Song, H. Dong, and Y. Hao, *Chinese J. Energ. Mater.*, 2000, **8**, 104-107.
34. Y. Zhang, G. Ji, F. Zhao, Z. Gong, D. Wei, L. Chen, and W. Li, *Mol. Simulat.*, 2011, **37**, 237-242.
35. R. H. Gee, A. Maiti, S. Bastea, and L. E. Fried, *Macromolecules*, 2007, **40**, 3422-3428
36. F. Li, L. Ye, F. Nie, and Y. Liu, *J. Appl. Polym. Sci.*, 2007, **105**, 777-782.
37. B. W. Cherry, Polymer Surfaces, Cambridge University Press: London, 1981.
38. S. Wu, Polymer Interface and Adhesion, Marcel Dekker Inc.: New York, 1982.
39. F. Nie and J. Sun, In the 3rd International Autumn Seminar on Propellants, Explosive and Pyrotechnics, 1999.
40. C. Lin, J. Liu, Z. Huang, F. Gong, Y. Li, L. Pan, J. Zhang, and S. Liu, *Propell. Explos. Pyrot.*, 2015, accepted.
41. Y. Li and M. R. Kessler, *Polymer*, 2014, **55**, 2021-2027.
42. F. Achereiner, K. Engelsing, M. Bastian, and P. Heidemeyer, *Polym. Test.*, 2013, **32**, 447-454.
43. F. C. Chang, F. Lam, and J. F. Kadla, *Mech. Time-Depend. Mat.*, 2013, **17**, 427-437.